Magnetic and electric hyperfine interactions in the rare-earth indium compounds R_2In studied by ^{111}Cd perturbed angular correlations

M. Forker* and R. Müßeler
Helmholtz-Institut für Strahlen- und Kernphysik der Universität Bonn, Nussallee 14-16, Bonn D-53115, Germany

S. C. Bedi
Department of Physics, Panjab University, Chandigarh, India

M. Olzon-Dionysio and S. Dionysio de Souza
Departamento de Fisica da Universidade Federal de São Carlos, São Carlos, São Paulo, Brazil
(Received 4 October 2004; published 4 March 2005)

The magnetic and electric hyperfine interactions of the probe nucleus ^{111}Cd on the In site of the ferromagnetic rare-earth (R) indium compounds R_2In (R=Pr, Nd, Sm, Gd, Dy, Ho, Er, and Tm) have been investigated by perturbed angular correlation (PAC) spectroscopy. In the paramagnetic phase, the axially symmetric quadrupole interaction (QI) decreases by more than a factor of 20 from R=Pr to R=Er indicating a significant influence of the $4f$ electrons on the charge distribution at the In site. In the ferromagnetic phase, the spin and temperature dependence of the magnetic hyperfine field B_{hf} and its orientation relative to the c axis of hexagonal R_2In have been determined by measuring the combined magnetic and electric hyperfine interaction as a function of temperature for all R constituents. The sign of B_{hf}, determined by applying an external field of 4 T, is positive for light and negative for heavy R_2In. The comparison of the ^{111}Cd hyperfine fields in R_2In and in R metals suggests that the indirect $4f-4f$ coupling is mediated by intra-atomic $4f-5d$ exchange and $5d-5d$ interaction of neighboring R atoms rather than by $4f$ exchange with the s-conduction electrons. The spin dependence of the saturation value of $B_{hf}(0)$ and of the Curie temperature in R_2In reflect a substantial difference of the $f-d$ exchange parameter Γ between the light (LR=Pr, Nd, Sm) and the heavy (HR=Gd, Tb, ...) R_2In compounds: $\Gamma_{LR}/\Gamma_{HR}=1.5(1)$. The deviation of the magnetic hyperfine field from its saturation value at low temperatures can be explained by the excitation of spin waves. In Gd_2In, the low temperature decrease of B_{hf} follows Bloch's $T^{3/2}$ relation. In the other R_2In compounds with nonzero angular momentum of the R constituent, the temperature dependence of B_{hf} is best described by the modified power law $T^{3/2}\exp(-\Delta/k_BT)$ which suggests the existence of an energy gap of about $\Delta/k_B\approx 15-20$ K in the spin wave spectrum of these anisotropic ferromagnets. With the exception of Pr_2In and Nd_2In, where the hyperfine field vanishes discontinuously at the Curie temperature, the magnetic phase transitions of R_2In are of second order. A critical increase of the linewidth of the magnetic interaction close to the phase transition indicates a spatial variation of the exchange interaction with a spread of the Curie temperature of about 2–5 K. The temperature-induced changes of the orientation of the $4f$ spins relative to the c axis of R_2In have been deduced from the angle between B_{hf} and the symmetry axis of the electric field gradient.

DOI: 10.1103/PhysRevB.71.094404 PACS number(s): 76.80.+y, 75.50.−y

I. INTRODUCTION

Measurements of magnetic and electric hyperfine interactions (hfi) are a useful tool for the investigation of magnetically ordered compounds. Electron spin polarizations, unquenched orbital angular moments, and magnetic dipole moments can give rise to magnetic hyperfine fields B_{hf} at nuclei in magnetic compounds. These hyperfine fields provide information on the exchange interactions leading to spontaneous magnetic order, on the order of magnetic phase transitions, on spin wave excitations, on relaxation processes, and on other parameters characterizing a magnetic system. They can be determined by measuring their interaction with known nuclear magnetic moments using techniques such as NMR, Mössbauer spectroscopy, perturbed angular correlations (PAC), and μSR. Additional information, *e.g.*, on the orientation of the magnetic moments or on magnetoelastic distortions, can frequently be obtained from the nuclear electric quadrupole interaction (QI) between the quadrupole moment of the nuclear probe and an electric field gradient (EFG) which arises if the charge distribution surrounding the probe site has noncubic symmetry.

The magnetic systems investigated by hyperfine spectroscopic techniques range from the pure $3d$ and $4f$ elemental ferromagnets to ordered and disordered intermetallics, inorganic compounds, amorphous alloys, nanocrystalline materials, etc. Much of the experimental and theoretical hyperfine interaction work has been focused on magnetic systems involving the rare earth (R) elements Ce to Tm.[1] Because these elements differ in the number of well-shielded $4f$ electrons, they have rather similar chemical properties. The $4f$ spins, which play a decisive role in the exchange interactions, and the orbital contributions to the $4f$ magnetic moments, however, vary strongly with the number of $4f$ electrons. Consequently, one finds a large number of isostructural series of R compounds that—for different R constituents—differ only

 ©2005 The American Physical Society

slightly in the crystallographic properties, but strongly in the magnetic properties and thus offer very favorable conditions for the separation of the magnetic from other solid-state parameters.

There are numerous hyperfine interaction studies of intermetallic compounds of rare earths with other elements.[2] In most of these studies, the hyperfine interaction is observed at impurity nuclei or the nuclei of the non-rare-earth constituents. At the R nuclei (except Gd) one has huge magnetic fields and electric field gradients, caused by the unquenched orbital angular momentum of the $4f$ shell and a precise determination of the much smaller contributions to the hyperfine interaction produced by the magnetic host may become difficult. Intermetallic compounds of the rare earths with $3d$ transition elements have attracted much interest because of the coexistence and interaction of highly localized ($4f$) and itinerant ($3d$) electrons. Hyperfine interaction studies of intermetallic compounds of rare earth and sp elements have frequently been aiming at information on the mechanism of the indirect exchange, which couples the spins of the localized nonoverlapping $4f$ electrons.

In the present work, we have used the probe nucleus ^{111}Cd for a PAC investigation of the magnetic and electric hyperfine interactions in the rare-earth indium compound R_2In that is part of a systematic study of intermetallic compounds of rare earth and sp elements. Apart from R_2In, the R-In phase diagram presents several other intermetallic compounds,[3] offering not only the possibility to vary the magnetic constituent in a given structure, but also to study the magnetic properties of different structures with the same R element.

The particular choice of In rather than another sp constituent for such a systematic investigation is related to the experimental technique employed: In most PAC and some Mössbauer studies, the probe nucleus is an impurity in the investigated compound, which raises the question of the lattice site occupied by the probe atom. Sometimes the hyperfine parameters provide an answer to this question, but frequently the probe site and the site preference (in cases of several nonequivalent lattice sites) cannot be determined from the hyperfine parameters alone, which leads to obvious difficulties for the interpretation of the experimental data. This problem does not arise in ^{111}Cd PAC studies of In compounds. The excited states of ^{111}Cd, one of the most favorable nuclei for PAC measurements, are populated by the electron capture decay of the radioisotope ^{111}In. Although the decay makes the daughter isotope ^{111}Cd an impurity in In compounds, the probe site is well known because the recoil caused by the electron capture decay is far too small to dislocate the isotope from its lattice position.

In the following, we report a series of PAC measurements of the magnetic and electric hyperfine interactions of ^{111}Cd on In sites of R_2In, carried out for R=Pr, Nd, Sm, Gd, Dy, Ho, Er, and Tm as a function of temperature in the range $10\ \mathrm{K} \leqslant T \leqslant 300\ \mathrm{K}$. Results for Tb_2In have been published previously.[4] The questions addressed in this study are the spin dependence of the magnetic hyperfine field, the influence of the R constituent on the temperature dependence of B_{hf}, the order of the magnetic phase transitions, the spin orientation and its changes with temperature, and the variation of the EFG at the In site across the R_2In series.

II. CRYSTAL STRUCTURE AND MAGNETIC PROPERTIES OF R_2In

The crystal structure of R_2In reported by Palenzona[5] and Franceschi[6] is isomorphous with the hexagonal Ni_2In lattice. The unit cell contains two structurally different R sites and one In site which has 11 R atoms at different distances d_n as nearest neighbors (NN). There are 6 NN R atoms at $d_1 = (c^2/16 + a^2/3)^{1/2}$, 2 NN R atoms at $d_2 = c/2$, and 3 NN R atoms at $d_3 = a/\sqrt{3}$. Both lattice parameters a and c ($a = 0.5534$ nm, $c = 0.6893$ nm for R=Pr) decrease linearly with increasing R atomic number, a slightly stronger than c. The ratio c/a therefore increases from $c/a = 1.246$ for R=Pr to $c/a = 1.255$ for R=Tm.[5]

The magnetic properties of R_2In have been investigated by magnetization and resistivity measurements,[7–9] by neutron diffraction,[10] and by ^{119}Sn Mössbauer spectroscopy.[11,12] In the paramagnetic phase, all R_2In (except Sm_2In) show Curie-Weiss behavior of the susceptibility with effective moments close to the free-ion values and positive paramagnetic Curie temperatures ($\theta_p \leqslant 197$ K).[9] In the magnetically ordered phase the susceptibility of R=Sm, Gd, Tb, and Dy indicates a transition from ferromagnetic to antiferromagnetic order as temperature is decreased. Gd_2In presents a metamagnetic transition at $T = 99.5$ K. For R=Ho, Er, and Tm the susceptibility shows a maximum at intermediate temperatures without giving an indication of the type of magnetic order.

The neutron diffraction studies of R_2In carried out for R=Gd, Tb, Er (Ref. 10) indicate a ferromagnetic structure below T_C with the $4f$ moments on both R sites close to the free-ion value. In the antiferromagnetic structure of Gd_2In below 100 K, the spins are perpendicular to the hexagonal c axis. Gd_2In presents a helicoidal structure with all spins in a given basal plane parallel to each other and a spiral angle between subsequent planes of about 60° at 20 K. Tb_2In is ferromagnetic down to 45 K with the $4f$ moments in the basal plane. At lower temperatures, a small helicoidal component is observed. Er_2In also presents a ferromagnetic structure with the magnetic moments tilted out of the basal plane by an angle of 13(5)° independent of temperature. At 1.6 K, indications of a helicoidal component have been found.

III. EXPERIMENTAL DETAILS

A. Sample preparation and equipment

The PAC measurements were carried out with the 171–245 keV cascade of ^{111}Cd, which is populated by the electron capture decay of the 2.8 d isotope ^{111}In. In the first step of the source preparation, In metal was doped with radioactive ^{111}In (concentration $\sim 10^{-8}$). For this purpose, trace amounts of ^{111}In were solute extracted with ethylic ether from a commercially available aqueous solution of $^{111}InCl_3$ and deposited on a thin In foil. It was found that the radioactivity could be reduced to the metallic state either by melt-

ing the foil in a hydrogen atmosphere or by diffusion, heating the In foil to 400 K for 1 h. The metallic state was confirmed by taking a PAC spectrum of the doped foil. Both procedures lead to the well-known PAC spectrum of ^{111}Cd in In metal. Most of the investigated samples were produced using the simpler diffusion process. In the second step of the sample preparation, the doped In was arc-melted in an argon atmosphere with the rare-earth metals in the stoichiometric ratio.

R_2In compounds are known to rapidly oxidize in air.[5] To avoid degradation, the samples (metallic spheres of about 30 mg) were not ground to a powder, but immediately after production transferred to the vacuum of a closed-cycle He refrigerator which was used to cool them to $10\ \mathrm{K} < T \leqslant 300\ \mathrm{K}$. The temperature was stabilized to about 0.1 K. The PAC measurements were carried out with a standard 4-detector BaF_2 setup.

Inactive samples of R_2In with R=Pr, Nd, Sm, Gd, Dy, Ho, Er, and Tm were characterized by x-ray diffraction measurements. The compounds were ground to a powder in an argon atmosphere and mixed with water-free silicon grease. In all cases except Pr_2In, the diffraction pattern of the Ni_2In structure reported by Palenzona[5] was observed. Contaminations by foreign phases were not detected. Pr_2In was found to oxidize very rapidly even under the silicon grease cover and only slight indications of the diffraction peaks were observed.

B. Data analysis

The angular correlation of two successive γ rays of a γ-γ cascade, expressed by angular correlation coefficients $A_{kk,}$ $(k=2,4)$ may be modulated in time by hyperfine interactions in the intermediate state of the cascade. For polycrystalline samples, this modulation can be described by the perturbation factor $G_{kk}(t)$ which depends on the multipole order, the symmetry and time dependence of the interaction, and on the spin of the intermediate state (for details see, e.g., Frauenfelder and Steffen[13]). For a static hyperfine interaction, the perturbation factor can be written as a sum of oscillatory terms:

$$G_{kk}(t) = s_{k0} + \sum_n s_{kn}\cos(\omega_n t)\exp\left(-\tfrac{1}{2}\delta\omega_n t\right). \qquad (1)$$

The frequencies ω_n are associated with the energy differences between the hyperfine levels into which the nuclear state is split by the hyperfine interaction. Except for a few simple cases where analytical expressions for the perturbation factor are available, the frequencies ω_n and the amplitudes s_{kn} have to be determined by diagonalization of the interaction Hamiltonian. The number of terms in Eq. (1) depends on the spin I of the intermediate state. The exponential factor accounts for possible distributions of the static hyperfine interaction caused by structural, chemical, and other defects, which lead to an attenuation of the oscillatory PAC pattern. The parameter δ is the relative width of a Lorentzian distribution.

Frequently, several fractions of nuclei subject to different hyperfine interactions are found in the same sample. The effective perturbation factor is then given by

$$G_{kk}(t) = \sum_i f_i G^i_{kk}(t). \qquad (2)$$

f_i (with $\Sigma_i f_i = 1$) is the relative intensity of the ith fraction.

In magnetically ordered R_2In the probe nuclei ^{111}In/^{111}Cd are subject to a magnetic hyperfine field and an EFG related to the noncubic point symmetry of the In site. The hyperfine field interacts with the nuclear magnetic moment and the EFG with the nuclear electric quadrupole moment Q of the intermediate state of the cascade. In the most general case, the theoretical perturbation function for a combined magnetic and electric hyperfine interaction depends on five interaction parameters and on the nuclear spin I. The interaction parameters are the magnetic frequency $\nu_M = g\,\mu_N B_{hf}/h$ (g represents the nuclear g factor, μ_N the nuclear magneton), the quadrupole frequency $\nu_q = eQV_{zz}/h$, the asymmetry parameter $\eta = (V_{xx}\text{-}V_{yy})/V_{zz}$, and the Euler angles θ and φ which describe the relative orientation of the magnetic hyperfine field and the EFG tensor. $V_{ii} = \delta^2 V/\delta i^2 (i = \mathrm{x,y,z})$ are the principal-axis components of the EFG tensor with $|V_{xx}| \leqslant |V_{yy}| \leqslant |V_{zz,}|$.

As expected from the crystal structure and confirmed by the PAC spectra of the paramagnetic phase (see below), the EFG at the In site of the R_2In is axially symmetric ($\eta=0$) with respect to the c axis. In this case, the energy eigenvalues of the combined interaction are independent of the Euler angle φ, and for a given nuclear spin I the perturbation factor depends on only three parameters: ν_M, ν_q, and the angle θ between B_{hf} and the symmetry axis of the EFG.

The number of independent parameters, which can be extracted from the PAC spectra of ^{111}Cd:R_2In is further reduced by the fact that in most R_2In compounds the magnetic interaction is much stronger than the quadrupole interaction. (See below.) For $\nu_M \gg \nu_q$ the eigenvalues of the Hamiltonian are to first order given by $E_M = h\nu_M + C_{l,m} h\nu_q (3\cos^2\theta - 1)$ and consequently the quadrupole frequency ν_q and the angle θ cannot be determined independently by a measurement of the interaction energies. In most cases, the experimental results are therefore expressed in terms of the magnetic interaction frequency ν_M, the quadrupole parameter $\nu_q^\theta = (3\cos^2\theta - 1)\nu_q$, and the relative width δ of the hfi distribution.

IV. MEASUREMENTS AND RESULTS

PAC spectra $A_{22}G_{22}(t)$ of ^{111}Cd in R_2In spectra were recorded for the constituents R=Pr, Nd, Sm, Gd, Dy, Ho, Er, and Tm as a function of temperature between 10 K and 300 K. The hyperfine parameters of ^{111}Cd:Tb_2In are given in Ref. 4.

The Curie temperatures derived from the present PAC data differ considerably from those found in the ^{119}Sn Mössbauer study of R_2In (Refs. 11 and 12) (see below) in which the samples had a Sn content of about 0.5%. To investigate to which extent this relatively high concentration of Sn impurities (compared to the In concentration of $\sim 10^{-8}$) affects the order temperature, the ^{111}Cd PAC measurements were extended to $Gd_2In_{0.95}Sn_{0.05}$.

The sign of the magnetic hyperfine field was determined for R=Nd, Sm, Gd, Dy, and Tm by applying an external

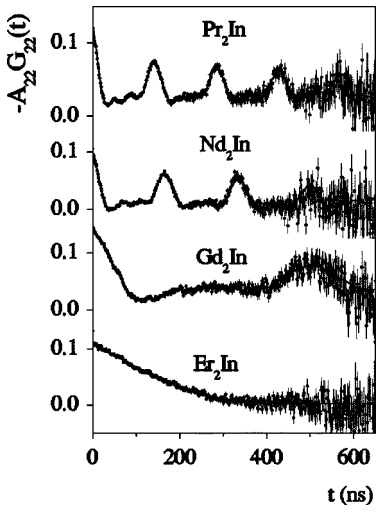

FIG. 1. PAC spectra of ^{111}Cd in the paramagnetic phase of some R_2In at 290 K.

magnetic field of 4 T at 4.2 K and observing the rotation of the integral angular correlation in a time-window of 3 ns. In the light R_2In, R=Nd, Sm the hyperfine field was found to be positive, i.e., parallel, in the heavy R_2In, R=Gd, Dy, Tm negative, i.e., antiparallel to the external field. For a comparison with R_2In, the measurements were extended to some rare-earth metals (Sm, Gd, Dy). As in R_2In, the sign of the ^{111}Cd hyperfine field is positive in light (Sm) and negative in heavy (Gd, Dy) R metals.

A. The quadrupole interaction of ^{111}Cd in paramagnetic R_2In

Some of the ^{111}Cd PAC spectra $A_{22}G_{22}(t)$ observed in the paramagnetic phase of R_2In at 290 K are shown in Fig. 1. For the light constituents R=Pr, Nd the spectra show the periodic modulation of the anisotropy typical for a perturbation by a well-defined axially symmetric QI ($\eta \leqslant 0.1$). As one moves from the light to the heavy R_2In, the strength of QI decreases drastically: The precession period in Gd_2In is more than 3 times larger than in Pr_2In and at the end of the R_2In series it has increased to the point that only the initial decrease of the anisotropy fits into the 600-ns-time window of ^{111}Cd. The values of the quadrupole frequency derived from these spectra are listed in Table I. In the analysis ν_q, η and δ were treated as free fit parameters. As a measure of the temperature dependence of the QI, Table I also gives the quadrupole frequency ν_q at $T \sim 1.05\ T_C$ in the paramagnetic phase close to the transition. In most cases, the asymmetry parameter was $\eta \leqslant 0.15$, with the exception of Pr_2In. In this compound, the asymmetry parameter increased substantially with decreasing temperature. Close to magnetic phase transition, one has $\eta = 0.45$. The relative linewidth δ of the QI distribution was found to increase across the R_2In series from $\delta \approx 0.07$ for Pr_2In to $\delta \approx 0.3$ at the end of the series. In the case of Er_2In the QI is too weak—compared to the time range available—for a determination of η and δ. The quadrupole frequency of Er_2In is therefore subject to a systematic uncertainty of the order of 100%. Some of the R_2In spectra showed a second component [$\nu_q \approx 100$ MHz, $\eta \approx 0$, relative intensity less than 10%] indicating a slight contamination by a nonidentified phase.

B. Combined magnetic and electric hyperfine interactions of ^{111}Cd in the magnetically ordered phases of R_2In

The PAC spectra observed in the magnetically ordered phase of R_2In at 10 K are collected in Figs. 2 and 3. There are noticeable differences between the spectra of the heavy (Fig. 2) and the light (Fig. 3) R_2In. Typically, the spectra of the heavy constituents R=Gd, Dy, Ho, Er, and Tm show a large number of periodic oscillations (with the corresponding frequency decreasing from R=Gd to Tm), with the oscillation amplitudes slowly modulated in time. The periodic oscillations are caused by the magnetic interaction; the amplitude modulations reflect the much weaker QI ($\nu_M \gg \nu_q$). For the light constituents R=Pr, Nd, Sm one observes nonperiodic modulation patterns, indicating that the ratio between the electric quadrupole and the magnetic dipole interaction in the light R_2In is larger than in the heavy R_2In. This is consistent with the increase of the QI observed in the paramag-

TABLE I. Experimental hyperfine interaction parameters of ^{111}Cd in R_2 In: The magnetic interaction frequency $\nu_M(0)$, the coefficient B, and the energy gap Δ/k_B [see Eq. (8)] derived from the low temperature variation of the magnetic frequency $\nu_M(T)$, the Curie temperature T_C, the quadrupole parameter $\nu_q^\theta = (3\cos^2\theta - 1)\nu_q$ at 10 K, the quadrupole frequency ν_q in the paramagnetic phase at 290 K and close to the magnetic phase transition ($T \approx 1.05\ T_C$).

R	$\nu_M(0)$(MHz)	$B(10^{-4}\ \mathrm{K}^{2/3})$	Δ/k_B(K)	T_C (K)	ν_q^θ(MHz)	ν_q(290 K)(MHz)	ν_q(T $\approx 1.05\ T_C$)(MHz)
Pr	20(1)			54	ν_q=38(1)	38.3	64.7; η=0.45
Nd	39.6	4.3(2)	22(3)	104	ν_q=54.5(5)	32.5	48.6
Sm	51.0	4.0(1)	54(3)	163	68(1)	26.3	34.5
Gd	72.1	2.7(1)		191	22.0(5)	13.1	17
Tb	59.6	3.5(1)	13(4)	163	9.0(5)	11.7(2)	15.7
Dy	51.7	5.8(3)	20(5)	122	17.0(5)	10.3(1)	14.3
Ho	40.6	11.4(2)	15(2)	83	16.5(5)	$7_{(+2,-5)}$	13.8
Er	26.3	29(2)	13(2)	43	10.7(5)	$1.5_{(+1,-1.5)}$	8.3
Tm	15.4	159(35)	15(3)	17	4.8(3)		

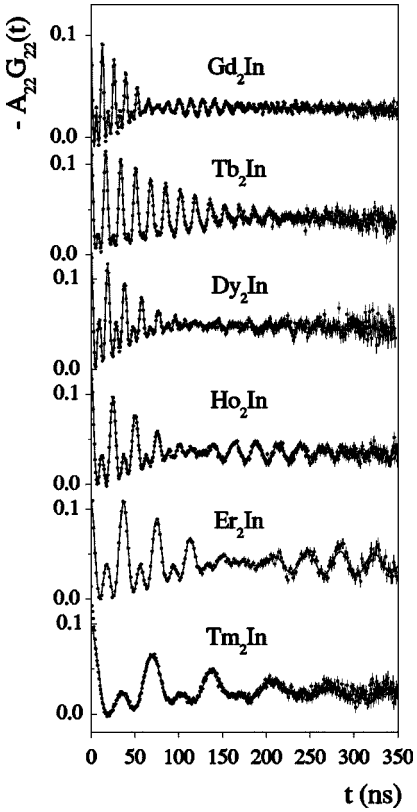

FIG. 2. PAC spectra of ^{111}Cd in heavy R_2In; R=Gd, Tb, Dy, Ho, Er, Tm at 10 K.

netic phase from Er_2In to Pr_2In. The parameters of the magnetic and electric hyperfine interaction and the relative width δ of the Lorentz distribution were extracted by fitting the theoretical perturbation function for a combined interaction to the measured spectra. Based on the results for the paramagnetic phase, it was assumed that the QI in the ferromagnetic phase has axial symmetry.

For R=Gd, Dy, Ho, Er, Tm, and Sm, one has $\nu_M > \nu_q$ and therefore only the quadrupole parameter $\nu_q^\theta = (3\cos^2\theta - 1)\nu_q$ could be determined unambiguously. The value of $\nu_M(0)$, extrapolated from the temperature dependence of the magnetic hyperfine frequency (see Sec. V B 1), and ν_q^θ at 10 K are listed in Table I. The Lorentz width δ, which in the magnetically ordered phase mainly describes the distribution of the magnetic hyperfine field, was of the order of $\delta \leqslant 0.03$ in

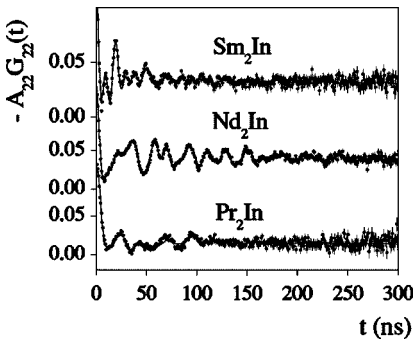

FIG. 3. PAC spectra of ^{111}Cd in light R_2In; R=Pr, Nd, Sm at 10 K.

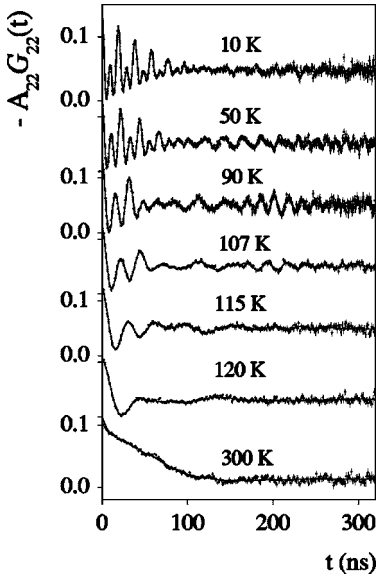

FIG. 4. PAC spectra of ^{111}Cd in Dy_2In at different temperatures.

all compounds, also those with a large distribution of the QI in the paramagnetic phase.

The typical evolution with temperature of the PAC spectra in magnetically ordered heavy R_2In is illustrated in Fig. 4, using $Dy_2In(T_C = 122\ \text{K})$ as an example. One feature of these spectra merits particular attention: As one approaches the order temperature, the oscillations of the anisotropy at times $t > 100$ nsec are increasingly attenuated and finally completely wiped out. (See the 120 K spectrum in Fig. 4,) This behavior, which has been observed in all heavy R_2In, reflects a critical increase of the Lorentzian linewidth δ close to T_C. The linewidth δ and the magnetic hyperfine frequency ν_M derived from the spectra in Fig. 4 are shown in Fig. 5 as a function of temperature.

In the paramagnetic phase, the QI is expressed by the quadrupole frequency ν_q, in the magnetically ordered phase by the quadrupole parameter $\nu_q^\theta = (3\cos^2\theta - 1)\nu_q$. The variation of these parameters with temperature for ^{111}Cd in Dy_2In is shown in the lower section of Fig. 6. The magnetic hyper-

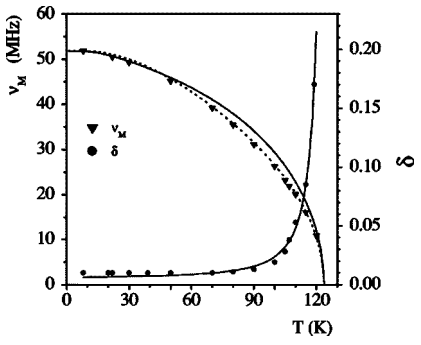

FIG. 5. The temperature dependence of the magnetic hyperfine frequency of ^{111}Cd (full triangles) in Dy_2In (left-hand scale). The solid line corresponds to the molecular-field magnetization calculated for the angular momentum $J = 15/2$ of Dy^{3+}. The full circles show the relative linewidth δ of the magnetic hyperfine field (right-hand scale).

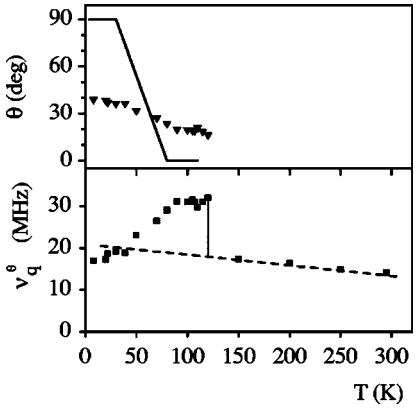

FIG. 6. The quadrupole frequency ν_q and the parameters $\nu_q^\theta = (3\cos^2\theta - 1)\nu_q$ of ^{111}Cd in the paramagnetic and the ferromagnetic phase, respectively, of Dy_2In as a function of temperature. The upper section shows the angle θ between the direction of B_{hf} and the symmetry axis of the EFG in ferromagnetic Dy_2In, derived from the experimental values of $\nu_q^\theta(T)$ (lower section), assuming that the temperature dependence $\nu_q(T)$ measured in the paramagnetic phase can be extrapolated to the ferromagnetic region (dashed line in the lower section). The solid line in the upper section corresponds to the temperature dependence of the angle θ, derived from the quadrupole interaction of the probe ^{119}Sn in Dy_2In. (Ref. 11).

fine frequencies $\nu_M(T)$ of all heavy R_2In compounds investigated in this study are collected in Fig. 7.

As an example of the temperature dependence of the ^{111}Cd PAC spectra in the light R_2In, we show in Fig. 8 a series of spectra observed in Nd_2In. These present several interesting aspects. One is the observation that the amplitude of the PAC pattern in the paramagnetic phase, which is a measure of the fraction of the sample in the paramagnetic state, decreases continuously as one approaches the magnetic phase transition at $T_C = 104$ K from higher temperatures and finally gives way to the nonperiodic pattern of the ferromagnetic phase. Such behavior is evidence for a coexistence of the paramagnetic and the ferromagnetic phases in a small temperature interval around the magnetic order transition (Ref. 14). The spectra of ^{111}Cd:Nd_2In (Fig. 8) close to T_C

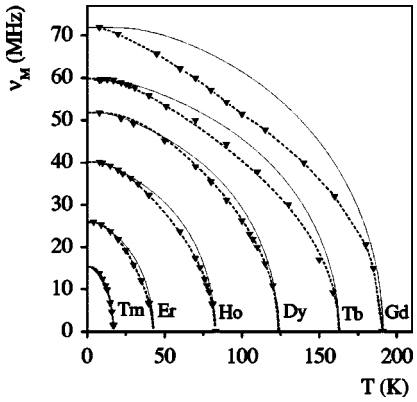

FIG. 7. The temperature dependence of the magnetic hyperfine frequency of ^{111}Cd in heavy R_2In; R=Gd, Tb, Dy, Ho, Er, Tm. The solid lines represent the molecular-field magnetizations, calculated for the respective angular moment J of the R constituents. The dotted lines are to guide the eyes.

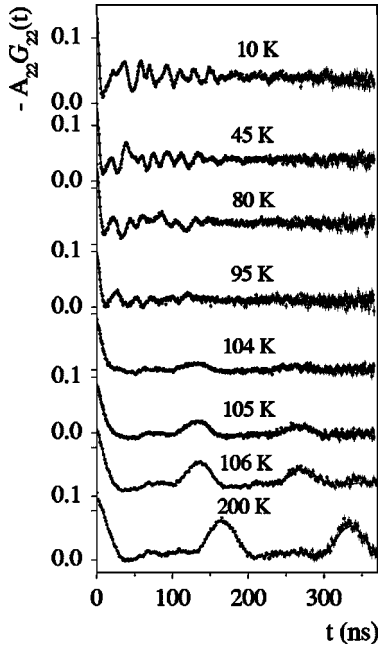

FIG. 8. PAC spectra of ^{111}Cd in Nd_2In at different temperatures.

were therefore analyzed assuming two fractions of probe nuclei, one with the relative intensity f_{para} describing probes in the paramagnetic phase, the other one with intensity $(1\text{-}f_{para})$ describing probes in the ferromagnetic phase. The resulting variation of the paramagnetic fraction with temperature is shown in the lower section of Fig. 9.

The second interesting aspect of Nd_2In—and Pr_2In—concerns the order of the magnetic phase transition.

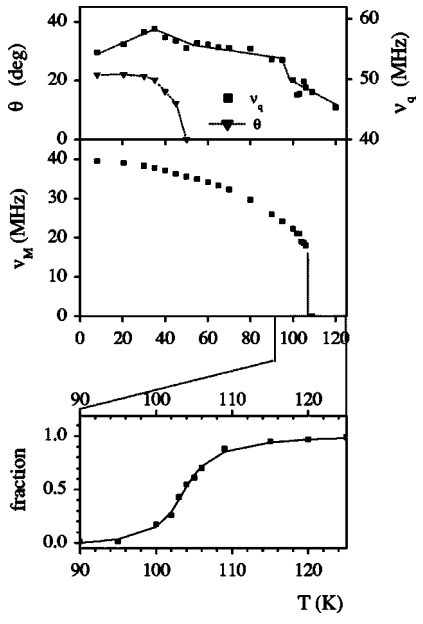

FIG. 9. The magnetic interaction frequency ν_M, the quadrupole frequency ν_q, and the angle θ between the magnetic hyperfine field and the symmetry axis of the EFG of ^{111}Cd in Nd_2In as a function of temperature. The bottom section shows the temperature dependence of the ferromagnetic fraction in the vicinity of the magnetic first-order transition at $T_C = 104$ K.

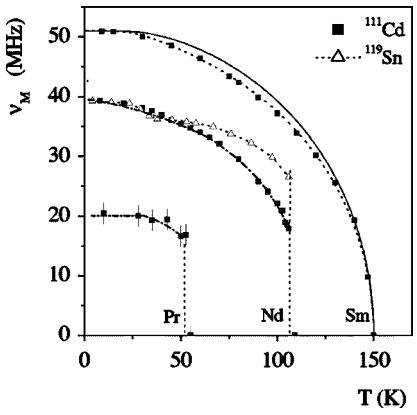

FIG. 10. The temperature dependence of the magnetic hyperfine frequency of ^{111}Cd in light R_2In; R=Pr, Nd, Sm. The solid line represents the molecular-field magnetization of Sm, calculated with the angular moment $J=5/2$ of Sm^{3+}. The open triangles represent the hyperfine interaction of the probe nucleus ^{119}Sn in Nd_2In [normalized to $\nu_M(0)$ of ^{111}Cd]. The dotted lines are to guide the eyes.

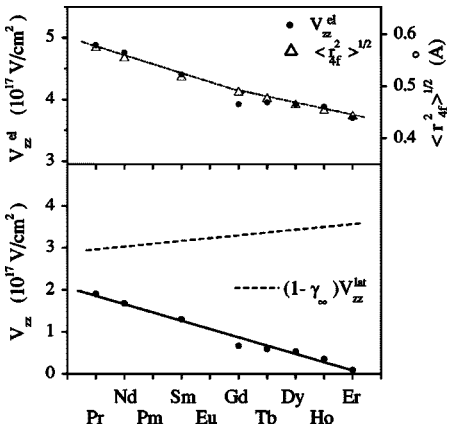

FIG. 11. The variation of the electric field gradient (EFG) V_{zz} of ^{111}Cd in R_2In at 290 K (full circles in the lower section), calculated from the measured quadrupole frequency ν_q. The dotted line in the lower section shows the lattice contribution to the EFG for the In charge state $Z=+2$. The full circles in the upper section represent the electronic contribution V_{zz}^{el} to the EFG, estimated from the measured values and the calculated lattice contribution. The open triangles in the upper section correspond to the root mean square radius $\langle r_{4f}^2 \rangle^{1/2}$ of the $4f$-wave function.

Figure 10 displays the temperature dependence of the magnetic hyperfine frequency of ^{111}Cd in the light R_2In, R=Pr, Nd, and Sm. While the transition in Sm_2In is of second order—as in the heavy R_2In compounds—the hyperfine field in Nd_2In and Pr_2In vanishes discontinuously at the transition temperature, indicating a first-order transition (FOT). The PAC observation of a FOT in Nd_2In agrees with the result of the ^{119}Sn Mössbauer study of this compound. For a comparison, the Mössbauer data extracted from Ref. 11 are included in Fig. 10.

In Sm_2In, the QI is still much weaker than the magnetic interaction and therefore only the QI parameter $\nu_q^\theta = (3\cos^2\theta - 1)\nu_q$ can be derived from the measured spectra. In the light Pr_2In and Nd_2In, however, one no longer has $\nu_q \ll \nu_M$ and therefore the quadrupole frequency ν_q and the angle θ between the symmetry axis of the EFG and B_{hf} can be separated in the analysis. The temperature dependence of the angle θ of Nd_2In is shown in the topmost section of Fig. 9. In the case of Pr_2In, the analysis with respect to the angle θ is complicated by the fact that, as one approaches the phase transition, the QI shows a considerable asymmetry which introduces the Euler angle φ as an additional parameter. With the asymmetry parameter fixed to the value in the paramagnetic phase close to T_C, the spectra of the ferromagnetic phase, which are practically independent of temperature, are compatible with an angle $\theta \leqslant 10°$.

V. DISCUSSION

A. The electric field gradient of ^{111}Cd in R_2In

The electric field gradient (EFG) V_{zz} of ^{111}Cd in R_2In at 290 K, calculated from the measured quadrupole frequency ν_q (see Table I) with the quadrupole moment $Q=0.80(10)b$ of the 245 keV state,[15] decreases strongly with increasing R atomic number from $V_{zz}=2.0(2)\times10^{17}$V/cm^2 for Pr_2In to $V_{zz}=0.15\times10^{17}$ V/cm^2 for Er_2In. This decrease cannot be explained by the variation of the lattice parameters a and c across the R_2In series. Because of the lanthanide contraction both a and c decrease slightly from Pr to Tm. The resulting variation of the EFG has been estimated by calculating the lattice contribution V_{zz}^{lat} in a point-charge model. The contributions of the R and the In sublattice to the total EFG can be expressed in terms of $(1-\gamma_\infty)V_{zz}^{lat}/Z$, where $(1-\gamma_\infty)=30$ is the Sternheimer correction[16] for Cd^{2+} and Z the charge state of the R and In ions, respectively. Between Pr_2In and Er_2In the contributions $(1-\gamma_\infty)V_{zz}^{lat}/Z$ of the R and In sublattices vary from −1.28 to −1.52 and from +0.44 to +0.49 (in units of 10^{17}V/cm^2), respectively. While it appears safe to use $Z_R=+3$ for the R ions, the charge state of the In ions is less obvious. Since the electronegativity of In is slightly larger than that of the R elements, one would expect that the In charge state in R_2In has a smaller value than in In metal ($Z_{In}=+3$). ^{155}Gd Mössbauer studies of the isomer shift in Gd_2In (Ref. 17) suggest a charge transfer of 0.25 s-electrons/Gd from Gd to In. To explain the trend of the EFG of ^{111}Cd in RIn_3, Mishra *et al.*[18] had to assume $Z_{In}=+1$. In Fig. 11 we compare the measured EFG V_{zz} to the lattice EFG $(1-\gamma_\infty)V_{zz}^{lat}$ calculated for the In charge state $Z=+2$ (dotted line in the lower section of Fig. 11). The comparison shows that the lanthanide contraction produces a slight increase of $(1-\gamma_\infty)V_{zz}^{lat}$ across the R_2In series. Other In charge states lead to the same trend, but different absolute values of $(1-\gamma_\infty)V_{zz}^{lat}$. The strong decrease of the measured EFG with increasing R atomic number must therefore be attributed to changes of the valence and conduction electron contribution to the EFG. As *ab initio* calculations of the EFG in R_2In are not available, we write the total EFG—for a qualitative discussion—as a sum of a lattice and an electronic contribution,

$$V_{zz} = (1-\gamma_\infty)V_{zz}^{lat} + V_{zz}^{el}. \tag{3}$$

Assuming that the two contributions have opposite signs, as suggested by the systematic of impurity EFG's in noncubic

metals,[19] the trends of the experimental EFG and of $(1-\gamma_\infty)V_{zz}^{lat}$ in Fig. 11 imply that the electronic part V_{zz}^{el} decreases strongly with increasing R atomic number. The variation of V_{zz}^{el}, derived from the experimental EFG for the In charge $Z_{In}=+2$, is shown in the upper section of Fig. 11. As the number of $4f$ electrons is the main parameter changing between Pr and Er, this variation is likely to be related to changes in the properties of the $4f$ electrons. Remarkably, the Z dependence of the electronic EFG contribution is very similar to that of the root mean square $4f$ radius, which characterizes the radial extension of the $4f$ wave function. (See open triangles connected by the dashed line in the upper section of Fig. 11, values of $\langle r_{4f}^2\rangle^{1/2}$ taken from Ref. 20.) Both quantities show a strong decrease in the group of the light R and a much weaker variation in the group of the heavy R. This similarity between the radial extension of the $4f$ wave function and the contribution V_{zz}^{el} to the EFG suggests that the EFG at the In site of R_2In is sensitive to the $4f$ charge distribution, possibly by overlap of the probe valence electrons with the $5d$ and $6s$ electrons of the rare earths which are hybridized by the interaction with the $4f$ shell.

The QI of ^{119}Sn in R_2In (Ref. 11) shows a completely different behavior. The EFG values scatter between $V_{zz}\sim 0$ for Er_2In and $V_{zz}\sim 7.3\ 10^{17}$ V/cm^2 for Gd_2In [calculated with $Q=-0.061(3)b$ (Ref. 21)] without a pronounced difference between light and heavy R_2In or any other systematic trend. This is remarkable since the data available on the EFG's of the probe nuclei ^{111}Cd and ^{119}Sn in the same noncubic metal[22] show that the ^{119}Sn EFG is systematically larger than the ^{111}Cd EFG by about a factor of 3. The reason for the drastically different EFG trends of ^{111}Cd and ^{119}Sn in R_2In is presently not clear. Although the site occupied by the probes has not been identified experimentally, there is no reason to assume that ^{119}Sn and ^{111}Cd are on different positions in R_2In.

Precise data on the temperature dependence of the ^{111}Cd QI in the paramagnetic phase of R_2In could be obtained only for R=Nd, Sm, Gd, Tb, and Dy. The values of $(\partial \ln \nu_q/\partial T)_{|300\ \mathrm{K}}$ cover a small range, extending from $-31(1)10^{-4}$ K^{-1} for R=Gd, Tb to $\sim -25\ 10^{-4}$ K^{-1} for R=Nd, Sm, Dy. A quite different behavior has been reported for ^{111}Cd in the rare-earth metals.[23] Here $(\partial \ln \nu_q/\partial T)_{|300\ \mathrm{K}}$ is about a factor of 2 smaller and shows a strong linear decrease with increasing R atomic number.

B. The magnetic hyperfine interaction

1. The spin dependence and sign of the saturation field $B_{hf}(0)$

The magnetic hyperfine field at the nuclei of non-rare-earth atoms in magnetically ordered compounds is caused by the Fermi contact term in the nucleus-electron interaction and reflects the spin polarization of the s electrons $\Delta\rho=[\rho\uparrow(0)-\rho\downarrow(0)]$ at the probe nucleus. A finite s-electron spin density may arise from the spin polarization of the host conduction electrons, the polarization of the electron core of the probe by a localized spin, and the overlap of the valence electrons of the probe with spin polarized valence electrons of the magnetic ions.

Because of the small spatial extension of the $4f$ electrons, magnetic order in rare-earth compounds requires a mechanism of indirect exchange between the $4f$ electrons. Mainly two mechanisms of indirect $4f-4f$ coupling have been proposed: In the Ruderman-Kittel-Kasuya-Yosida (RKKY) theory the coupling is mediated by the s-conduction electrons, which are spin polarized by exchange with the $4f$ electrons. In an alternative concept, which was proposed by Campbell,[24] the indirect coupling is provided by intra-atomic $4f-5d$ exchange and interatomic $5d-5d$ interaction between the spin polarized $5d$ electrons of neighboring R atoms. In spite of considerable experimental and theoretical effort, a clear picture of the indirect coupling in intermetallic compound RM_x of rare earths and sp elements has not yet emerged. There is experimental evidence that, e.g., in RM (M=Cu, Ag, Mg) and $R\mathrm{In}_3$ the indirect coupling is mainly mediated by sp electrons,[25] but in a number of cases the experimental data are partially in conflict with the RKKY formalism and suggest that the $5d$-electrons play an important role in the indirect exchange interaction.[2]

In the RKKY theory, a spin located at position R_n induces a spatially nonuniform spin polarization in a sea of free conduction electrons,

$$P(r) = -\frac{9n^2\pi\Gamma}{2E_F}\langle S_z\rangle F(2k_F|r-R_n|). \tag{4}$$

E_F and k_F are the free-electron Fermi energy and wave vector, respectively. Γ is an effective s-f exchange constant (assumed to be independent of the electron wave vector), and $F(x)=[x\cos(x)-\sin(x)]/x^4$ is the oscillating RKKY function. The spin polarization induced by spin $\vec{S}_n$ interacts with a second spin $\vec{S}_m$ localized at R_m. The resulting indirect coupling can be described by the Hamiltonian $H_{nm}=-j_{nm}\vec{S}_n\cdot\vec{S}_m$. As the total angular momentum J rather than the spin S is the constant of motion, the spin has to be substituted by its projection $(g-1)J$ on the total angular momentum J (Ref. 26), leading to $H_{\mathrm{nm}}=-j_{nm}(g-1)^2\,J(J+1)$. In the RKKY theory, the interaction constant j_{nm} is proportional to the square of the s-f exchange parameter Γ and the RKKY function $j_{nm}\propto\Gamma^2F(2k_FR_{nm})$, so that the Curie temperature is proportional to[27]

$$T_C\propto\Gamma^2(g-1)^2J(J+1). \tag{5}$$

The indirect coupling via intra-atomic $4f-5d$ exchange and $5d-5d$ interaction can be described phenomenologically by the same Hamiltonian. In this coupling scheme, Γ would be a measure of the $4f-5d$ exchange and the long-range RKKY function has to be replaced by a function which adequately accounts for the radial dependence of the $5d-5d$ interaction.

As long as orbital angular momentum contributions to the spin polarization[28,29] are excluded, one therefore expects in both coupling schemes the hyperfine field to be proportional to the $4f$ spin and the respective exchange parameter Γ. In the case of RKKY coupling, all $4f$ spins contribute so that

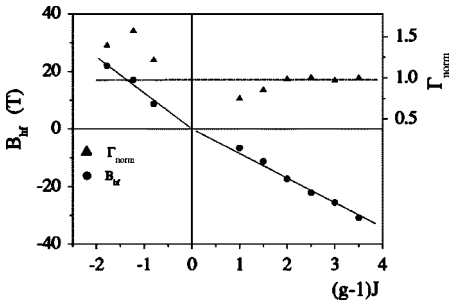

FIG. 12. The spin dependence of the magnetic hyperfine field of ^{111}Cd in R_2In (full circles, left-hand scale) and the relative coupling constant $\Gamma_{norm} \propto B_{hf}/(g-1)J$ (triangles, right-hand scale) with the normalization $\Gamma_{norm}(\mathrm{Gd})=1$.

$$B_{hf} \propto C\Gamma(g-1)J\sum_{n\neq m} F(2k_F R_{nm}). \tag{6}$$

The parameter C accounts—in the case of impurity probes—for the modification of the host's s-electron spin polarization by spin-dependent electron scattering at the impurity potential.[30] In the case of intra-atomic $4f-5d$ exchange, the hyperfine field is produced by the overlap of the spin polarized $5d$ electrons with the valence electrons of the probe. Since the $5d$ electrons are more strongly localized than the s electrons, one would expect that the hyperfine field is mainly determined by the number N of nearest R neighbors and their distance R_i to the probe. Even without detailed knowledge of the radial dependence, it can be presumed that the contributions of the NN spins, symbolized by $f(R_i)$, increase with decreasing distance R_i Qualitatively, these factors can be summarized by the expression,

$$B_{hf} \propto C\Gamma(g-1)J\sum_{i=1}^{N} f(R_i). \tag{7}$$

Equations (6) and (7) show that independent of the details of the coupling mechanism, the spin dependence of the hyperfine field in a series of isostructural compounds of rare earths and sp elements reflects the R dependence of the effective exchange parameter Γ, provided the R positions vary only slightly across the series. This is the case for R_2In where the lanthanide contraction changes the lattice parameters between $R=$Pr and $R=$Tm by less than 5%. In Fig. 12 we have therefore plotted the saturation values $B_{hf}(0)$ of the magnetic hyperfine field of ^{111}Cd in R_2In, calculated from the experimental values of $\nu_M(0)$ (Table I) with the nuclear g factor $g=0.301$, versus the spin projection $(g-1)J$. Both for the group of the light and the heavy R constituents, one observes in a first approximation a linear relation between B_{hf} and the spin projection. The slopes of these relations, which with the above assumptions are a direct measure of the exchange parameter Γ, however, differ considerably between both groups. A fit of linear relations to the experimental data leads to a ratio $\Gamma_{LR}/\Gamma_{HR}=1.5(1)$, where Γ_{LR} and Γ_{HR} are the exchange parameters for the light (Pr, Nd, Sm) and the heavy (Gd, Tb, …, Tm) R_2In compounds, respectively. The conclusion that the effective exchange in the light R_2In is substantially stronger than in the heavy compounds is also supported

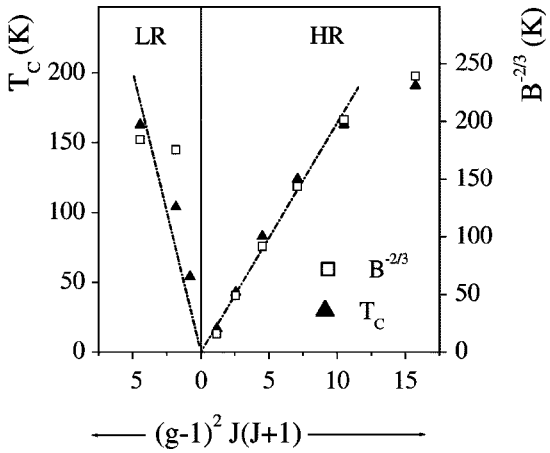

FIG. 13. The Curie temperature T_C (full triangles, left-hand scale) and the quantity $B^{-2/3}$ (open squares, right-hand scale) as a function of the de Gennes factor $G=(g-1)^2J(J+1)$. B is the coefficient of the $T^{3/2}$ term in Eq. (8). The right section shows the data of the heavy rare earths $HR=$Gd, Tb, Dy, Ho, Er, Tm, the left section those of the light $LR=$Sm, Nd, Pr.

by the order temperatures T_C of the R_2In series. The variation of T_C of R_2In (see column 5 in Table I) as a function of the de Gennes parameter $G=(g-1)^2J(J+1)$ shown in Fig. 13 is approximately linear with clearly different slopes Γ^2 for the light and the heavy R_2In. Excluding $T_C(\mathrm{Gd_2In})$ which fits poorly into the linear trend, one obtains the ratio $\Gamma_{LR}/\Gamma_{HR}=1.70(25)$, or including $T_C(\mathrm{Gd_2In})$ the ratio is $\Gamma_{LR}/\Gamma_{HR}=1.55(25)$. Within the errors, both values agree with $\Gamma_{LR}/\Gamma_{HR}=1.5(1)$ deduced from the spin dependence of B_{hf}. Numerous other intermetallic compounds of rare earths and sp elements present similar differences. From the order temperatures of $R\mathrm{Al_2}$ and RCd, e.g., one estimates $\Gamma_{LR}/\Gamma_{HR}=1.7$. The $B_{hf}/(g-1)J$ values of ^{119}Sn in $R\mathrm{Al_2}$ (Ref. 31) also differ considerably between the light and the heavy $R\mathrm{Al_2}$. One of the interpretations proposed[31] involves an orbital angular momentum contribution to the spin polarization. When attributed to different spin exchange constants only, the spin dependence of $B_{hf}(^{119}\mathrm{Sn}{:}R\mathrm{Al_2})$ corresponds to a ratio $\Gamma_{LR}/\Gamma_{HR}=1.45$.

For a closer inspection of the R dependence of the exchange parameter Γ in R_2In, the upper section of Fig. 12 shows the relative coupling constant $\Gamma_{norm}(R) \propto B_{hf}/(g-1)J$ with the normalization $\Gamma_{norm}(\mathrm{Gd})=1$. A strong change occurs between the light and the heavy R_2In, but the variations in each group are relatively weak. For most of the heavy R_2In, the ratios $B_{hf}/(g-1)J$ and $(T_C/G)^{1/2}$ (see columns 4 and 5 in Table II) are constant within a few percent, decreasing only at the end of the series. At this point, it is interesting to compare the hyperfine fields of ^{111}Cd in R_2In to those of the probe ^{119}Sn in the same series. The ^{119}Sn data taken from Ref. 11 are listed in Table III. The ratio of the hyperfine fields $B_{hf}(^{111}\mathrm{Cd})/B_{hf}(^{119}\mathrm{Sn})$ (see column 4 of Table III) is—within a few percent—constant across the R_2In series. This probe-independence strengthens the interpretation of the ratio $B_{hf}/(g-1)J$ as a relative measure of the effective exchange parameter of the host compound.

Some insight into the coupling mechanism may be gained by comparing the ^{111}Cd hyperfine field in R_2In to that in the

TABLE II. The spin dependence of the saturation value of the magnetic hyperfine field of ^{111}Cd in R_2In and in R metals. $(g-1)J$ is the projection of the spin on the total angular momentum J and $G=(g-1)^2J(J+1)$ is the de Gennes factor. $B_{hf}(R_2\mathrm{In})/B_{hf}(R)$ and $T_C(R_2\mathrm{In})/T_C(\mathrm{R})$ are the ratios of the ^{111}Cd hyperfine fields and of the Curie temperatures, respectively, of R_2In and the R metals.

		R_2In			R metal		
R	$(g-1)J$	B_{hf}(T)[a,b]	$B_{hf}/(g-1)J$(T)	$(T_C/G)^{1/2}$(K)$^{1/2}$	B_{hf}(T)	$\frac{B_{hf}(R_2\mathrm{In})}{B_{hf}(\mathrm{R})}$	$\frac{T_C(R_2\mathrm{In})}{T_C(R)}$
Pr	−0.8	$(+)8.6_5$	(−)10.8	8.2			0.16
Nd	−1.227	$+17.0_5$	−13.8	7.5	$(+)7.65_{15}$[c]	2.21	0.19
Sm	−1.786	$+21.9_5$	−12.2	6.0	$+24.2_6$[d,e]	0.90	0.67
Gd	3.5	-30.9_3	−8.8	3.5	-34.0_7[f,g]	0.91	0.65
Tb	3	-25.6_3	−8.5	4.1	$(-)27.5_5$[g]	0.96	0.71
Dy	2.5	-22.2_2	−8.9	4.1	-22.1_4[d,h]	1.00	0.69
Ho	2	$(-)17.4_2$	(−)8.7	4.3	$(-)14.9_3$[g]	1.14	0.67
Er	1.5	$(-)11.3_2$	(−)7.5	4.1	$(-)11.6_3$[g]	0.97	0.51
Tm	1	-6.6_1	−6.6	3.8	$(-)6.0_6$[g]	1.1	0.30

[a]This work.
[b]Reference 4.
[c]Reference 47.
[d]Sign: this work.
[e]Reference 48.
[f]Reference 49.
[g]Reference 50.
[h]Reference 51.

R metals, if one assumes comparable coupling parameters for a given R element. In R_2In, the probe nucleus has 11 nearest R neighbors at a slightly smaller average distance (Pr: 0.348 nm, Tm: 0.332 nm) than that of the 12 NN in the R metals (Pr: 0.367 nm, Tm: 0.354 nm). In the case $4f-5d$ exchange and $5d$-robe overlap, one would therefore expect a hyperfine field ratio of $B_{hf}(R_2\mathrm{In})/B_{hf}(R)=11/12=0.92$ or larger values in case of a strong radial dependence of $f(R_i)$ in Eq. (7). On the other hand, the free-electron RKKY sum $\Sigma_{n\neq m}F(2k_FR_{nm})$ of R_2In (Ref. 9) is roughly 2/3 of the RKKY sum of the R metals,[27] as one would expect if in a simplifying picture 1/3 of the magnetic R atoms are replaced by nonmagnetic In atoms.

In the case of ^{111}Cd (see column 7 of Table II) one finds a hyperfine ratio of $B_{hf}(R_2\mathrm{In})/\mathrm{B_{hf}}(R)\approx 0.9-1.1$ (except $R=$Nd) close to the ratio of the number of nearest R neighbors

TABLE III. The spin dependence of the saturation value of the magnetic hyperfine field of ^{119}Sn in R_2In (Refs. 11 and 12) and in R metals. The Curie temperatures of R_2 In have been derived from the temperature dependence of the magnetic hyperfine field of ^{119}Sn. $B_{hf}(^{111}\mathrm{Cd})/B_{hf}(^{119}\mathrm{Sn})$ is the ratio of the hyperfine fields of the probe nuclei ^{111}Cd and ^{119}Sn in R_2In, $B_{hf}(R_2\mathrm{In})/B_{hf}(R)$ the ratio of the hyperfine fields of ^{119}Sn in R_2In and in R metals.

	R_2In			R metal	
R	T_C(K)	B_{hf}(T)	$\frac{B_{hf}(^{111}\mathrm{Cd})}{B_{hf}(^{119}\mathrm{Sn})}$	B_{hf}(T)	$\frac{B_{hf}(R_2\mathrm{In})}{B_{hf}(\mathrm{R})}$
Nd	111	+21.9(1)	0.77		
Sm	160	(+)27.3(1)	0.79		
Gd	198[a], 236[b]	−37.3(1)	0.84	−32.34(4)[c]	1.16
Tb	172	−32.8(1)	0.81	(−)24.1(6)[d]	1.37
Dy	131	−27.1(1)	0.82	(−)18.5(5)[d]	1.47
Ho	91,5	(−)22.3(1)	0.76	(−)12(1)[d]	1.85
Er	50	(−)15.2(1)	0.74	−12.4(4)[e]	1.23
Tm	23, 5	−8.4(1)	0.79	(−)7.2(12)[d]	1.20

[a]Reference 11.
[b]Reference 12.
[c]Reference 52.
[d]Reference 53.
[e]Reference 54.

$N(R_2\mathrm{In})/N(R)=0.92$. For ^{119}Sn (see column 6 of Table III) the ratio is even larger: $B_{hf}(R_2\mathrm{In})/\mathrm{B_{hf}}(R)\approx 1.2-1.8$. Thus, for both probes $B_{hf}(R_2\mathrm{In})\mathrm{B_{hf}}(R)$ is much larger than the ratio of the RKKY sums ($\sim$0.60). This implies that the $4f$ spins beyond the NN shell of the probe contribute little to the hyperfine field and favors $4f-5d$ exchange and $5d$-probe interaction rather than long-range RKKY interaction as coupling mechanism. NMR measurements[32] of B_{hf} of ^{67}Zn in pseudobinary $R_{1-x}A_x\mathrm{Zn}$ (A=La, Y, Sc) have led to a similar conclusion. In these compounds, about 80% of the hyperfine field comes from the NN $4f$ spins. The fact that for ^{119}Sn the ratio $B_{hf}(R_2\mathrm{In})/\mathrm{B_{hf}}(R)$ is substantially larger than for ^{111}Cd is possibly related to the difference of the probe volumes. The atomic volume of Sn (27 Å^3) which is comparable to the volume of the Wigner Seitz cell of the In site of R_2In (Pr:29 Å^3; Er:26 Å^3) is larger than the atomic volume of Cd(22 Å^3) which could lead to a stronger overlap of the Sn valence electrons with the spin polarized $5d$ electrons.

The Curie temperatures of R_2In and R metals are related as $T_C(R_2\mathrm{In})\approx 2/3\ T_C(R)$ (at least for heavy R—see column 8 in Table II). This supports the picture of R_2In as a magnetically diluted R metal with a comparable exchange parameter, since in diluted ferromagnets above the percolation limit T_C scales with the concentration of the magnetic atoms, independent of the coupling mechanism.

The larger exchange parameter in the light R_2In deduced from the hyperfine field measurements reflects a higher degree of $4f-5d$ overlap which can be understood qualitatively by comparing the radial extensions of the $4f$ and $5d$ electrons in the first and the second half of the R series. According to Delyagin *et al.*,[11,33] the degree of overlap can be expressed by the ratio R_{4f}/R_{NN}. Here the root mean square $4f$ radius $R_{4f}=\langle r_{4f}^2\rangle^{1/2}$ and the NN distance R_{NN} are measures of the radial extensions of the $4f$- and the $5d$-wave functions, respectively. In an isostructural series, both parameters decrease with increasing Z. The decrease of R_{NN} (lanthanide contraction) between Pr and Tm usually amounts to only a few percent ($\sim$5% in R_2In). The $4f$ radius, however, shows a strong Z dependence, in particular in the first half of the rare-earth group where it decreases by about 20%. In the second half, the decrease is about 10%. (See the dotted line in the upper section of Fig. 11.) Consequently, the degree of overlap decreases from Pr to Tm, leading to weaker exchange in the second half of the R series.

The sign of the magnetic hyperfine field B_{hf} of ^{111}Cd on the In site of R_2In has been determined for R=Nd, Sm, Gd, Tb, Dy, and Tm. As a rule, in light R_2In B_{hf} is parallel, in heavy R_2In is antiparallel to the external field B_{ext}. An external field of 4 T is not sufficient to break the spin-orbit coupling of the R moments; the external field therefore aligns the total angular momentum J. According to Hund's rule, for light R elements the spin S is antiparallel, and for heavy R it is parallel to the total angular momentum. The positive and negative sign of B_{hf} in light and heavy R_2In, respectively, therefore implies that in all R_2In the spin polarization $\Delta\rho_i=[\rho\uparrow(0)-\rho\downarrow(0)]$ at the ^{111}Cd site is antiparallel to the rare-earth spin S. The same holds for the rare-earth metals, and as shown by Delyagin *et al.*,[11] also for the probe nucleus ^{119}Sn in R_2In.

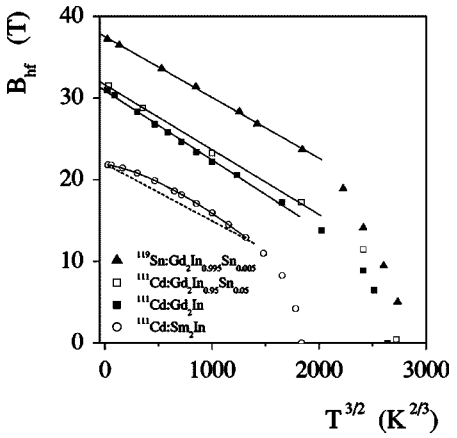

FIG. 14. The magnetic hyperfine field B_{hf} of ^{111}Cd in Gd_2In (full squares), in $Gd_2In_{0.95}Sn_{0.05}$ (open squares), in Sm_2In (open circles), and of ^{119}Sn in $Gd_2In_{0.995}Sn_{0.005}$ (full triangles; Ref. 12), as a function of temperature on a $T^{3/2}$ scale. The full line through the ^{111}Cd:Sm_2In data is the result of a fit of Eq. (8) to the experimental values.

2. The temperature dependence of the magnetic hyperfine interaction

The variation of the magnetic interaction frequency ν_M with temperature was determined in all R_2In between 10 K and the order temperature T_C. The main results of the measurements are illustrated in Figs. 5, 7, 10, and 14. In all heavy R_2In, the magnetic hyperfine interaction decreases continuously towards T_C. The decrease of ν_M is accompanied by a critical increase of the linewidth of the magnetic interaction, which is evidence for a spatial variation of the exchange interaction and a corresponding distribution of the Curie temperature. (See Sec. V B 3).

In light R_2In, a second-order transition (SOT) is found only in Sm_2In. In Nd_2In and Pr_2In the hyperfine field vanishes discontinuously at the Curie temperature. The observation that the QI in the paramagnetic phase of Pr_2In becomes axially asymmetric as one approaches the phase transition (see Section IV A) is an indication of lattice distortions near T_C and suggests that these first-order transitions (FOTs) are driven by magneto-elastic effects.

In Fig. 7, the temperature dependence of $\nu_\mathrm{M}(T)$ of ^{111}Cd in heavy R_2In compounds is compared to the prediction of a molecular field model for localized moments (solid lines). For all heavy R_2In, the experimental trend of $\nu_\mathrm{M}(T)$ is slightly below the molecular field curve. It is interesting to note that in spite of the phase transitions from antiferromagnetic to ferromagnetic order in Gd_2In and Sm_2In at 100 K and 145 K, respectively, the hyperfine frequencies of ^{111}Cd (and ^{119}Sn, Ref. 11) in these hosts vary smoothly across the phase transitions. As pointed out by Delyagin *et al.*,[11] the absence of a singularity of B_{hf} suggests that the NN spin arrangements in the ferro- and antiferromagnetic phases are rather similar and calls for a small interlayer turn angle of the spin spirals of Gd_2In and Sm_2In.

At low temperatures, the excitation of spin waves causes the magnetization to deviate from its saturation value, which is frequently expressed in terms of a temperature power law

T^{κ}. The $T^{3/2}$ temperature dependence of the magnetization predicted by Bloch's spin wave theory for a bilinear Heisenberg ferromagnet with nearest-neighbour interactions has been experimentally verified in a large number of cases, but other exponents κ have also been observed.[34]

In Fig. 14 we have plotted the magnetic hyperfine field of ^{111}Cd in Gd_2In and Sm_2In vs the temperature on a $T^{3/2}$ scale. Clearly, $B_{hf}(T)$ of ^{111}Cd in Gd_2In is well described by a $T^{3/2}$ relation, but substantial deviations from Bloch's law occur in Sm_2In and the other R_2In compounds (not shown in Fig. 14) with nonzero orbital angular momentum. An analysis of the temperature dependence of the magnetic hyperfine frequency $\nu_M(T)$ of ^{111}Cd in R_2In in terms of a single temperature power law T^{κ} leads to significant differences in the exponent κ. A fit of $(1\text{-}BT^{\kappa})$ to the data in Fig. 7 for $T/T_C \leqslant 0.5$ results in $\kappa = 1.45(5)$ for Gd_2In, $\kappa = 1.65(5)$ for Tb_2In and $1.8 \leqslant \kappa \leqslant 2.2$ for the other R constituents.

Similar differences between Gd and the other rare-earth elements have been observed in the thermal decrease of the magnetization of the pure R metals. In Gd metal,[35] the low-temperature variation of the magnetization for $T/T_C \geqslant 0.17$ is well described by a $T^{3/2}$ relation. In Tb[36] and Dy,[37] however, larger critical exponents $\kappa \approx 2-2.5$ are required to reproduce the decrease of the magnetization with a single temperature power law. These differences in the low-temperature trend of the magnetization have been attributed to the differences in the crystal electric field interactions (CEF) of Gd and the other rare-earth elements. In contrast to the other R elements, the charge distribution of the half-filled $4f$ shell of Gd is almost spherically symmetric. In Gd compounds, the anisotropic CEF interactions between the $4f$-charge distribution and the electric field produced by the surrounding charges are therefore weak, while for the other R elements one finds extremely large anisotropy energies. It was pointed out by Niira[37] that a magnetic anisotropy caused, e.g., by a CEF interaction may produce an energy gap Δ in the magnon spectrum of a ferromagnetic system[38] and that such a gap has a substantial effect on the low-temperature dependence of the magnetization.

For hcp rare-earth metals, the CEF can be expressed in terms of the anisotropy energies $K_l^0(l=2,4,6)$ relative to the hexagonal c axis and the basal plane anisotropy K_6^6. In this case, the CEF leads to an energy gap $\Delta \approx (1/J)\sqrt{K_2^0 K_6^6}$ in the spin wave spectrum and the resulting modification of Bloch's $T^{3/2}$ law can be written as[38]

$$M(T) = M(0)\left[1 - BT^{3/2}\sum_{n=1}^{\infty} n^{2/3}\exp(-n\Delta/k_BT)\right]. \quad (8)$$

With energy gaps of about $\Delta/k_B \approx 20-30$ K, Eq. (8) fully accounts for the deviations of the low-temperature magnetization of Tb and Dy metal from Bloch's $T^{3/2}$ relation.

Because of the hexagonal symmetry of R_2In, substantial CEF effects should be present for all R constituents except R=Gd and one may therefore expect similar differences in the temperature dependence of the magnetization as in the R metals. We have analyzed the experimental temperature dependencies of $\nu_M(T)$ in the range for $T/T_C \leqslant 0.5$ on the basis of Eq. (8). This analysis, which presumes that the hyperfine coupling constant A relating the hyperfine field to the magnetization[39] $[\nu_M(T) = AM(T)]$ is temperature independent, leads to a finite parameter Δ/k_B for all non-S state R constituents. The values of $\nu_M(0)$, B and Δ/k_B derived from a fit of Eq. (8) to the $\nu_M(T)$ data in Figs. 7 and 10 are listed in columns 2–4 of Table I. In the case of Pr_2In, the accuracy of the data (see Sec. IV B) is insufficient for a meaningful analysis of the temperature dependence.

In the heavy R_2In, the gap energy $\Delta/k_B \approx 15(3)$K is practically independent of the R constituent and of the same order of magnitude as the magnon gap of Tb and Dy metals. In the light R_2In R=Nd, Sm, the gap energy is substantially larger, reflecting a stronger CEF interaction which is probably a consequence of the larger radial extension of the $4f$-wave functions in first half of the $4f$ series. In contrast to the gap energy, the parameter B of the temperature dependence [Eq. (8)] shows a strong variation with the R constituent, increasing continuously from $B = 2.7 \times 10^{-4}$ K$^{-3/2}$ for Gd to $B = 159 \times 10^{-4}$ K$^{-3/2}$ for Tm. In the spin wave theory of isotropic Heisenberg ferromagnets with Hamiltonian $\mathcal{H} = -\mathcal{J} S_1 S_2$ and three-dimensional dispersion relation, the relative deviation of the magnetization from its saturation value is for small wave vectors given by $\{[\Delta M(T)/[M(0)]\} \propto \{1/S)[(k_BT)/(\mathcal{J} S)]^{3/2}\}$. (Note: This proportionality also holds in the presence of anisotropy energies.[27]) The coupling parameter $\mathcal{J}$ may be replaced by the order temperature since $\mathcal{J} \propto T_C/S(S+1)$. This substitution leads to the relation $B^{-2/3} \propto T_c[S^{2/3}/(S+1)]$ between the coefficient B of the $(1\text{-}BT^{3/2})$ temperature dependence of the magnetization and T_C. [Note: In the case of the R ferromagnets, S stands for the spin projection $(g-1)J$]. In the range of spins of interest in this paper, $S^{2/3}/(S+1) \approx$ const ≈ 0.52 and one therefore expects a practically linear relation between the Curie temperature T_C and the parameter $B^{-2/3}$.

To compare our experimental observations with this prediction of the spin wave theory, we have included the parameter $B^{-2/3}$ (see Table I) in Fig. 13, where the Curie temperature T_C is plotted vs the de Gennes factor $G = (g-1)^2 J(J+1)$, and find that $B^{-2/3}$ indeed follows the G-dependence of the order temperature very closely. The experimental $B^{-2/3}$ values of all R_2In, except Nd_2In, satisfy the linear relation $B^{-2/3} = 2.34(4)\ T_C S^{2/3}/(S+1)$. In the case of Nd_2In, $B^{-2/3}$ is about 50% larger than expected from this relation, which is possibly related to the fact that the magnetic phase transition of Nd_2In is of first order.

For $T/T_C \leqslant 0.5$, the temperature-induced decrease of the magnetic hyperfine field of ^{111}Cd:R_2In can thus be consistently related to the spin wave excitations of the host. Our data also suggest that the response of the electron spin polarization to the spin wave excitations, described by the hyperfine coupling constant A, depends on the properties of the probe atom. In Fig. 14 we have included the $B_{hf}(T)$-data of ^{119}Sn in Gd_2In, extracted from Fig. 3 of Ref. 12. As for ^{111}Cd, $B_{hf}(T)$ of ^{119}Sn follows a $T^{3/2}$ law; the coefficient $B(^{119}\text{Sn}:Gd_2In) = 2.0(1) \times 10^{-4}$ K$^{2/3}$, however, is considerably smaller than that of ^{111}Cd in the same host $[B(^{111}\text{Cd}:Gd_2In) = 2.7\ 10^{-4}$ K$^{-3/2}]$.

At higher temperatures, the variation of the magnetic hyperfine field may be discussed in terms of the molecular field

model. For rare-earth ferromagnets, the CEF interaction changes the equidistant molecular field splitting of the $(2J+1)$ m states, and the Boltzmann averaging of these levels then results in a different temperature dependence of the magnetization. Including the Hamiltonian of a CEF interaction with hexagonal point symmetry into the molecular field model, we have found that anisotropy coefficients $K_2^0 \approx -(100-200)$ K and $K_4^0/K_2^0 \approx 0.1$ are required to reproduce the measured $\nu_M(T)$ curves of ^{111}Cd:R_2In (except Gd_2In). These values are comparable to the coefficients observed in the R metals. A precise determination of the coefficients is difficult because similar temperature dependences can be produced by different combinations of K_2^0 and K_4^0. This is because the magnetization is given by the Boltzmann average over all m states, in contrast, e.g., to inelastic neutron scattering which directly provides the m-state energies. The contributions of the K_6^0 and K_6^6 terms to CEF energy are too small to be detected in the $\nu_M(T)$ curves.

The Curie temperatures of most R_2In derived from the ^{111}Cd PAC measurements of $\nu_M(T)$ (see Tables I and III) are systematically smaller—by up to 10 K—than those obtained from the ^{119}Sn Mössbauer spectra (Table III). To investigate whether this difference is related to the Sn content ($\sim$0.5%) of the Mössbauer samples, we have measured $B_{hf}(T)$ of ^{111}Cd in $Gd_2In_{0.95}Sn_{0.05}$. These data, included in Fig. 14, show that there is some increase of the saturation field and of the order temperature upon addition of this relatively large Sn concentration. The effect, however, is too small to explain the substantial difference in the order temperatures deduced from the PAC and the Mössbauer spectra.

3. Evidence for Curie temperature distributions in R_2In

As pointed out in Sec. IV B, there are two features in the PAC spectra near T_C that reflect a spatial variation of the exchange interaction and a corresponding distribution of the order temperature in R_2In. These are (i) the critical increase of the relative line width of the magnetic hyperfine field (see Figs. 4 and 5, for example) and (ii) the coexistence of the paramagnetic and the ferromagnetic phase in a small temperature interval near T_C (Figs. 8 and 9). Evidence for Curie temperature distributions has earlier been found in disordered ferromagnetic systems. T_C spreads of the order of a few K, resulting in critical line broadening and phase coexistence near T_C have been observed by Mössbauer[40,41] and PAC (Ref. 42) spectroscopy in concentrated and dilute, disordered alloys. The concept of spatially varying Curie temperatures[43,44] has also been invoked to explain the smoothness of the phase transitions in strongly disordered magnetic alloys such as Invar where the transition may extend over temperature ranges of the order of 10^2 K. (See, for example, Ref. 45)

Recently, it was noted that distributions of the order temperature may also occur in chemically ordered intermetallic compounds.[14] A T_C distribution produces a critical increase of the linewidth, in particular at second-order transitions (SOT), because at low temperatures the magnetic frequency ν_M varies little with the Curie temperature, but close to T_C, ν_M decreases critically with decreasing T_C: $\nu_M \propto (1-T/T_C)^{\beta}$ with an exponent of the order $\beta \sim 0.3-0.4$[46]. At $T \approx T_C$ small variations of the Curie temperature therefore produce broad distributions of ν_M, while at low T the magnetic frequency remains sharply defined. As shown in Ref. 14, for a SOT with critical exponent β and a Lorentzian T_C-distribution, characterized by the center temperature T_C and the width Γ_C, the resulting temperature dependence of the relative line width δ is given by

$$\delta(T) = (\beta\,\Gamma_C/2T_C)(T/T_C)(1-T/T_C)^{\beta-1}. \tag{9}$$

The extraction of the parameter Γ_C from the critical increase of $\delta(T)$ is discussed in detail in Ref. 14 With the critical exponent β fixed to $\beta=0.35$ and a Curie temperature of $T_C=122(1)$K deduced from $\nu_M(T)$ of Dy_2In using $\nu_M \propto (1-T/T_C)^{\beta}$, the $\delta(T)$ data of Dy_2In in Fig. 5 correspond to a T_C-distribution with a line width of $\Gamma_C=1.8(2)$K. In the other R_2In compounds with SOTs, Γ_C is of the same order of magnitude.

A coexistence of the paramagnetic and the ferromagnetic phases near T_C becomes manifest in the PAC spectra as a superposition of two fractions. The temperature dependence of the paramagnetic fraction is given by the integral[14]

$$f_{para}(T) = \int_0^{\mathrm{T}} I(T_C';T_C)\,dT_C', \tag{10}$$

where $I(T_C';T_C)$ represents the T_C distribution (with T_C as most frequent order temperature). In the ferromagnetic phase of R_2In, the angular correlation is perturbed by a combined magnetic and electric hyperfine interaction, in the paramagnetic phase by an axially symmetric QI. The paramagnetic component in the spectra at $T \approx T_C$ is most easily identified in the case of ^{111}Cd:Nd_2In (see Fig. 8) because of the strength and the narrow linewidth of the QI in this compound. In the heavy R_2In, the QI is much weaker, and the paramagnetic component is therefore difficult to separate from the ferromagnetic component, which because of the critical increase of the line width is strongly attenuated at $T \approx T_C$. A fit of Eq. (10) with a Lorentzian T_C distribution to $f_{para}(T)$ of ^{111}Cd:Nd_2In (solid line in Fig. 9) gives $T_c=104$ K and a width of the T_C distribution of about $\Gamma_C \approx 5$ K. [Note: The variations of the sample temperature of $\sim$0.1 K are at least one order of magnitude smaller than the Γ_C values required to reproduce the temperature dependences of $\delta(T)$ and $f_{para}(T)$ at $T \approx T_C$.]

Critical increase of the linewidth and phase coexistence have been observed in practically all hyperfine field studies of chemically ordered magnetic compounds reported up to now. The mechanism leading to local variations of the exchange interaction in ordered systems has not yet been identified. Site disorder (atoms A on B sites of AB_x) probably plays a role.

4. The spin orientation

The relative orientation of the magnetic hyperfine field and the axially symmetric EFG reflects the local spin orientation at the probe with respect to the symmetry axis of the host lattice. With the exception of Nd_2In and Pr_2In, the information on the spin orientation at ^{111}In/^{111}Cd in R_2In has

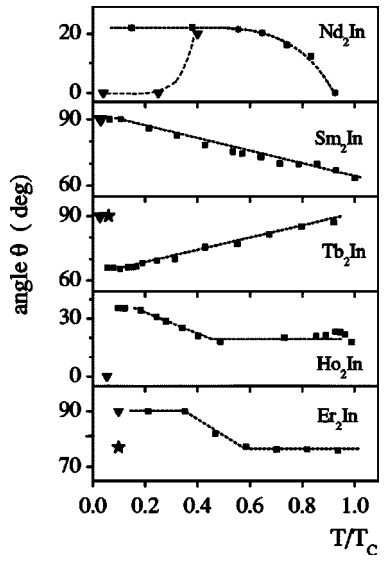

FIG. 15. The angle θ between the direction of the ^{111}Cd hyperfine field and the symmetry axis of the EFG (full squares) in some R_2In as a function of temperature. The full triangles are the θ values deduced from ^{119}Sn Mössbauer measurements (Ref. 11), the stars corresponds to the orientation of the $4f$ moments relative to the c axis determined by neutron diffraction (Ref. 10).

to be extracted from the quadrupole parameter $\nu_q^\theta = (3\cos^2\theta - 1)\nu_q$ by extrapolating the temperature dependence of the quadrupole frequency $\nu_q(T)$, measured in the paramagnetic phase, to the ferromagnetic region. An example is given in Fig. 6 for the case of Dy_2In. At T_C one has $|\nu_q^\theta = (3\cos^2\theta - 1)\nu_q| \sim 1.8|\nu_q|$ with $\theta \sim 16$ deg as the only solution. The decrease of $\nu_q^\theta(T)$ with decreasing temperature implies an increase of the angle θ. The variation of $\theta(T)$ shown in upper section of Fig. 6 results from the experimental values of $\nu_q^\theta(T)$ if the temperature dependence of the QI is assumed to follow the well known $T^{3/2}$-relation $\nu_q(T) = \nu_q(0)(1 - BT^{3/2})$ observed in many noncubic metals. As the variation of the QI in the paramagnetic phase is rather weak, the assumption of a linear $\nu_q(T)$ relation leads to practically the same $\theta(T)$ values. Figure 6 also shows the variation of $\theta(T)$ for a ^{119}Sn impurity on the In site of Dy_2In, measured by Mössbauer spectroscopy (full line in the upper section[11]).

The temperature dependencies of the spin orientation at ^{111}Cd derived in the same way from the experimental $\nu_q^\theta(T)$ data of the other R_2In compounds are displayed in Fig. 15 vs the reduced temperature T/T_C. Gd_2In and Tm_2In are not included. In the latter case the QI in the paramagnetic phase is very small and $\nu_q(T)$ too imprecise for a meaningful analysis of $\nu_q^\theta = (3\cos^2\theta - 1)\nu_q$. The decrease of quadrupole parameter with decreasing temperature, however, shows that also in Tm_2In the spin orientation changes with temperature.

In the case of Gd_2In, the quadrupole parameter of the ferromagnetic phase $\nu_q^\theta(T)$ is close to the quadrupole frequency extrapolated from the paramagnetic phase: $|\nu_q^\theta/\nu_q| \sim 1$ at all temperatures, but in Er_2In this ratio increases from $|\nu_q^\theta/\nu_q| \sim 0.9$ at T_C to $|\nu_q^\theta/\nu_q| \sim 1$ at $T = 10$ K. For $0.9 < |(3\cos^2\theta - 1)| < 1$ there are two possible solutions: $\theta \approx 35-37°$ and $\theta \geqslant 79°$. Since γ-γ PAC is not sensitive to the sign of the QI, one has to recur to data provided by other techniques to select the correct solution. Neutron diffraction and ^{119}Sn Mössbauer spectroscopy of R_2In support the solution $\theta \geqslant 79°$ both for R=Gd and Er.

The experimental error of $\nu_q^\theta(T)$ is of the order of 2%, so that qualitatively there is no doubt that the spin orientation in most R_2In—as seen by ^{111}Cd—is temperature dependent. The absolute values of θ obtained from $\nu_q^\theta(T)$, however, depend on the $\nu_q(T)$ relation assumed for the extrapolation from the paramagnetic to the ferromagnetic phase and are therefore the subject of some systematic uncertainty which we estimate to be of the order of $\Delta\theta \leqslant 10$ degrees.

For comparison with the ^{111}Cd PAC results, the spin orientations of R_2In obtained by neutron diffraction and ^{111}Sn Mössbauer spectroscopy are included in Fig. 6 (Dy_2In) and Fig. 15. In the case of ^{119}Sn Mössbauer spectroscopy, the information on the spin orientation comes, as for ^{111}Cd: R_2In, from the quadrupole parameter $\nu_q^\theta = (3\cos^2\theta - 1)\nu_q$. In contrast to γ-γ PAC, however, in the case of combined interactions Mössbauer spectra are sensitive to the sign of ν_q^θ. Delyagin *et al.*[11] have reported that for R=Sm, Gd, Tb, Dy, and Tm $\nu_q^\theta(^{119}\text{Sn}:R_2\text{In})$ at 4.2 K is positive, for R=Ho and Nd negative. The assumption of a positive sign of the EFG then leads to the conclusion that in the case of R=Sm, Gd, Tb, Dy, and Tm one has $\theta \geqslant \theta_M$, where θ_M is the "magic" angle $\theta_M = 54.7°$, i.e., the magnetic moments are in the basal plane or close to it. For R=Ho and Nd one has $\theta \leqslant \theta_M$, i.e., the moments are parallel or close to the c axis of the hexagonal R_2In lattice.

A temperature dependence of ν_q^θ has been reported only for the case of $^{119}\text{Sn}:Dy_2In$ where the sign of $\nu_q^\theta$was found to change from positive to negative, as temperature increased from 40 K to 80 K (indicated by the full line in the upper section of Fig. 6). In the case of $^{119}\text{Sn}:Nd_2In$ an anomaly in the temperature variation of the magnetic hyperfine field between 25 K and 40 K (see triangles connected by a dashed line in Fig. 10) has been attributed by Delyagin *et al.*[11] to a spin reorientation from $\theta = 0°$ to $\theta = 20°$. With ^{111}Cd, a similar anomaly has not been observed.

The comparison of the ^{111}Cd PAC, the ^{119}Sn Mössbauer, and the neutron diffraction results shows that the local spin orientation is affected by the probe properties, presumably by local changes of the crystal field parameters. Pronounced differences between neutron diffraction and PAC results are found, e.g., in the case of Tb_2In ($\theta = 90°$ and 65°, respectively, at 10 K; see Fig. 15). The results of ^{111}Cd PAC and ^{119}Sn Mössbauer spectroscopy differ in practically all R_2In compounds. A prominent example is Dy_2In (see Fig. 6): At the site of ^{119}Sn, the angle θ increases strongly with decreasing temperature from $\theta \sim 0°$ to 90°. At ^{111}Cd, the spin orientation changes in the same temperature range, but only from $\theta \sim 20°$ to $\sim 40°$. A low temperature angle of $\theta \sim 90°$ can be definitely excluded for ^{111}Cd, because on the way from $\theta \sim 20°$ to $\theta \sim 90°$ one would pass through the magic angle $\theta_M = 54.7°$ where the PAC pattern is that of a pure magnetic interaction. This has not been observed.

VI. CONCLUSION

The magnetic and electric hyperfine interactions of the probe nucleus ^{111}Cd on the In site of the ferromagnetic rare-

earth indium compound R_2In have been investigated by perturbed angular correlation measurements as a function of temperature for different R constituents. The main results of this study are summarized in the following paragraph.

The QI in the paramagnetic phase decreases drastically from the light to the heavy R constituents, suggesting a strong influence of the $4f$ electrons on the charge distribution at the In site. The comparison of the magnetic hyperfine field of ^{111}Cd in R_2In and in the R metals shows that the main contribution to B_{hf} comes from the nearest R neighbors of the probe. This observation favors intra-atomic $4f-5d$ exchange and interatomic $5d-5d$ interaction rather than $4f$ exchange with the s-conduction electrons as mechanism of the indirect $4f-4f$ interaction. The spin dependence of the hyperfine field reflects a stronger degree of $4f-5d$ overlap in the first half of the R group. The temperature dependence of the magnetic hyperfine interaction at $T/T_C \leqslant 0.5$ can be explained by the excitation of spin waves. For R constituents with nonzero orbital angular momentum, $B_{hf}(T)$ follows the modified Bloch relation $T^{3/2}\exp(-\Delta/k_BT)$), suggesting an energy gap $\Delta/k_B \approx 15-20$ K in the spin wave spectrum of R_2In. The PAC spectra provide evidence for a spatial variation of the exchange interaction in chemically ordered intermetallic compounds that is probably due to some degree of site disorder. The spatially varying exchange leads to a distribution of the Curie temperature with a width of $\sim 2-5$ K and to the coexistence of the ferromagnetic and the paramagnetic phase in a similar temperature interval around the phase transition. The temperature-induced changes of the orientation of the $4f$ spins relative to the c axis of R_2In have been deduced from the angle between B_{hf} and the symmetry axis of the EFG.

ACKNOWLEDGEMENT

Two of the authors (M.O.D and S.D.S) would like to express their gratitude for financial support by FAPESP, Brazil.

*Electronic address: forker@iskp.uni-bonn.de

[1] R. G. Barnes, in *Handbook of Chemistry and Physics of Rare Earths*, edited by K. A. Gschneidner and L. Eyring (North-Holland, Amsterdam, 1979), Vol. 2, Chap. 18.
[2] K. H. J. Buschow, in *Ferromagnetic Materials*, edited by E. P. Wohlfarth (North-Holland, Amsterdam, 1980), Vol. 1, Chap. 4.
[3] I. Iandelli and A. Palenzona, in *Handbook of Chemistry and Physics of Rare Earths*, edited by K. A. Gschneider and L. Eyring (North-Holland, Amsterdam, 1979), Vol. 2, Chap. 13.
[4] M. Olzon-Dionysio, S. Dionysio de Souza, R. Müßeler, and M. Forker, J. Phys.: Condens. Matter **4**, 4307 (1992).
[5] A. Palenzola, J. Less-Common Met. **16**, 379 (1968).
[6] E. Franseschi, J. Less-Common Met. **37**, 157 (1974).
[7] H. Gamari-Seale, T. Anagnostopoulos, and J. K. Yakinthos, J. Appl. Phys. **50**, 434 (1979).
[8] S. P. McAlister, J. Phys. F: Met. Phys. **14**, 2167 (1984).
[9] W. Bazela and A. Szytula, J. Less-Common Met. **138**, 123 (1988).
[10] D. Ravot, O. Gorochov, T. Roisnel, G. Andre, F. Boureevigneron, and J. A. Hodges, Int. J. Mod. Phys. B **7**, 818 (1993).
[11] N. N. Delyagin, G. T. Mujiri, and V. I. Nesterov, Sov. Phys. JETP **69**, 1070 (1989).
[12] N. N. Delyagin, G. T. Mujiri, V. I. Nesterov, and S. I. Reiman, Sov. Phys. JETP **59**, 592 (1984).
[13] H. Frauenfelder and R. M. Steffen in *Perturbed Angular Correlations*, edited by K. Karlsson, E. Matthias, and K. Siegbahn (North-Holland, Amsterdam, 1963).
[14] M. Forker, S. Müller, P. de la Presa, and A. F. Pasquevich, Phys. Rev. B **68**, 014409 (2003).
[15] H. Ernst, E. Hagn, and E. Zech, Phys. Lett. **93A**, 357 (1983).
[16] F. D. Feiock and W. R. Johnson, Phys. Rev. **187**, 39 (1969).
[17] H. de Graaf, R. C. Thiel, and K. H. J. Buschow, J. Phys. F: Met. Phys. **12**, 2079 (1982).
[18] S. N. Mishra, R. G. Pillay, K. Raghunathan, P. N. Tandon, S. H. Devare, and H. G. Devare, Phys. Lett. **91A**, 193 (1982).
[19] R. S. Raghavan, E. N. Kaufmann, and P. Raghavan, Phys. Rev. Lett. **34**, 1280 (1975).
[20] A. J. Freeman and J. P. Desclaux, J. Magn. Magn. Mater. **12**, 11 (1979).
[21] M. Grodicki, V. Manning, A. X. Trautwein, and J. M. Friedt, J. Phys. B **20**, 5595 (1987).
[22] R. Vianden, Hyperfine Interact. **35**, 1079 (1987).
[23] M. Forker, L. Freise, and D. Simon, J. Phys. F: Met. Phys. **18**, 823 (1988).
[24] I. A. Campbell, J. Phys. F: Met. Phys. **2**, L47 (1972).
[25] G. E. Grechnev, A. S. Panfilov, I. V. Svechkarev, K. H. J. Buschow, and A. Czopnik, J. Alloys Compd. **226**, 107 (1995).
[26] P. G. de Gennes, J. Phys. Radium **23**, 510 (1962).
[27] B. Coqblin, *The Electronic Structure of Rare-Earth Metals and Alloys: The Magnetic Heavy Rare-Earths* (Academic Press, London, 1977).
[28] B. D. Dunlap, I. Nowik, and P. M Levy, Phys. Rev. B **7**, 4232 (1973).
[29] E. Belorizky, J. J. Niez, and P. M. Levy, Phys. Rev. B **23**, 3360 (1981).
[30] E. Daniel and J. Friedel, J. Phys. Chem. Solids **24**, 1601 (1963).
[31] N. N. Delyagin, V. I. Krylov, N. I. Moreva, G. T. Mudzhiri, V. I. Nesterov, and S. I. Reiman, Sov. Phys. JETP **61**, 176 (1985).
[32] K. Eckrich, E. Dormann, A. Oppelt, and K. H. J. Buschow, Z. Phys. B **23**, 157 (1976).
[33] N. N. Delyagin and V. I. Krylov, Solid State Commun. **126**, 401 (2003).
[34] U. Köbler, J. Phys.: Condens. Matter **14**, 8861 (2002), and references therein.
[35] H. E. Nigh, S. Legvold, and F. H. Spedding, Phys. Rev. **132**, 1092 (1963).
[36] D. E. Hegland, S. Legvold, and F. H. Spedding, Phys. Rev. **131**, 158 (1963).
[37] K. Niira, Phys. Rev. **117**, 129 (1960).
[38] A. R. MacIntosh and H. Bjerrum Møller, in *Magnetic Properties of Rare Earth Metals*, edited by R. J. Elliott (Plenum Press, London, 1972), Chap. 5.

[39] E. P. Wohlfarth, in *Ferromagnetic Materials*, edited by E. P. Wohlfarth (North Holland, Amsterdam, 1980), Vol. 1, Chap. 1.
[40] G. S. Collins, A. R. Chowdhury, and C. Hohenemser, Phys. Rev. B **26**, 4997 (1982).
[41] X. S. Chang, C. Hohenemser, and L. Takacs, Phys. Rev. B **40**, 29 (1989).
[42] R. M. Suter and C. Hohenemser, in *Magnetism and Magnetic Materials-1975*, edited by J. J. Becker, G. H. Lander, and J. J. Rhyne, AIP Conf. Proc. No. 29 (AIP, New York, 1976), p. 493.
[43] A. Yu. Romanov, V. P. Silin, and D. Wagner, Phys. Lett. A **116**, 370 (1997).
[44] A. Yu. Romanov and V. P. Silin, J. Exp. Theor. Phys. **86**, 120 (1998).
[45] M. Shiga, K. Makita, K. Uematsu, Y. Muraoka, and Y. Nakamura, J. Phys.: Condens. Matter **2**, 1239 (1990).
[46] C. Hohenemser, N. Rosov, and A. Kleinhammes, Hyperfine Interact. **49**, 267 (1989).
[47] M. Forker, L. Freise, and D. Simon, Solid State Commun. **71**(12), 1167 (1989).
[48] M. Forker and L. Freise, Hyperfine Interact. **34**, 329 (1987).
[49] L. Boström, E. Karlsson, and S. Zetterlund, Phys. Scr. **2**, 65 (1970).
[50] M. Forker and A. Hammesfahr, Z. Phys. **263**, 33 (1973).
[51] M. Forker and A. Hammesfahr, Z. Phys. **260**, 13 (1973).
[52] S. I. Reiman, N. I. Rokhlov, V. S. Shpinel, and E. P. Kamiskaya, Sov. Phys. JETP **59**, 190 (1984).
[53] A. S. Kuchma and V. S. Shpinel, Sov. Phys. JETP **35**(3), 556 (1972).
[54] D. C. Price and R. Street, J. Phys. C **1**, 1258 (1968).